Influence of pH on moisture-absorbing swelling cracks of red layer in central Sichuan and its micro-mechanism

Kang Huang
Wuhan Institute of Rock and Soil Mechanics Chinese Academy of Sciences
Fei Yu
Wuhan Institute of Rock and Soil Mechanics Chinese Academy of Sciences
Zhe Zhou
Wuhan Institute of Rock and Soil Mechanics Chinese Academy of Sciences
Kaiwen Tong
Wuhan Institute of Rock and Soil Mechanics Chinese Academy of Sciences
Wei Zhang
Wuhan Institute of Rock and Soil Mechanics Chinese Academy of Sciences
Zhangjun DAI (zjdai@whrsm.ac.cn)
Wuhan Institute of Rock and Soil Mechanics Chinese Academy of Sciences https://orcid.org/0000-0003-4960-8941
Shanxiong Chen
Wuhan Institute of Rock and Soil Mechanics Chinese Academy of Sciences

Research Article

Keywords: expansion of mudstone hygroscopic fissures, digital speckle correlation method, various pH conditions, displacement field and strain field, expansion mechanism

Posted Date: April 27th, 2022

DOI: https://doi.org/10.21203/rs.3.rs-1531469/v1

Abstract

In this study, the characteristics of self-absorption cracking and its micro-mechanism in the dry state of red mudstone in central Sichuan in the southwestern region were examined using a self-designed water absorption device combined with the digital speckle correlation method (DSCM), scanning electron microscopy, X-ray diffraction experiments, mercury intrusion experiments, and other methods. The results indicated theta compared with an alkaline environment, an acidic environment resulted in the self-absorption and cracking of mudstone. The maximum water absorption rate of mudstone and fracture rate in a pH of 3 were determined as 15.77 and 18.909%, respectively; whereas for pH = 11, they were 11.71 and 7.111%, respectively. In the acidic environment, the maximum combined displacement value and maximum principal strain value of mudstone self-priming and swelling evolution were both greater than in an alkaline environment. Simultaneously, in the former, the moisture absorption failure characteristics of mudstone exhibited increased swelling strain zones and swelling cores. The three possible mechanisms by which pH affects the expansion of mudstone hygroscopic fissures were proposed: hydration-expansion softening, adsorption-wedge failure, and humidity stress field. However, it was found that the solutions with different pH values may affect these three microscopic mechanisms through the following four physical or chemical processes: mineral dissolution, ion absorption and exchange, particle association, and pore change. The results of this study are expected to be of significance and aid in roadbed design, tunnel support, slope treatment, and other projects in the southwest region.

1. Introduction

The total area of red beds in China is approximately 820,000 km2. with the red beds in Southwest China accounting for 33% of the country’s total area, which is the region with maximum presence of red beds (Huang et al., 2005; Guo et al., 2007). A red layer is a type of clastic rock strata deposited under the effect of high continental temperature following oxidation owing to the environment with red as the primary colour, and mainly formed during the Jurassic and Cretaceous (Zhong et al., 2019; Dai et al., 2020). The red beds are primarily composed of mudstone, sandy mudstone, and sandstone. Among these, mudstone exhibits the worst engineering properties, such as low strength, brittle nature, and easily softens, disintegrates, and weathers away when in contact with water. Further, it exhibits expansibility and significant rheology (Yang et al., 2006; Chen et al., 2009). In study mudstone acquired from Sichuan Province, Neijiang City, Zizhong County, and belonging to the Middle Jurassic Xintiangou Formation was studied. The red mudstone can absorb moisture and expand, resulting in the generation, expansion, and penetration of cracks. Consequently, it has resulted in several engineering disasters, such as the deformation of the upper arch of the roadbed, rupture of the tunnel floor, and instability and collapse of the slope.

In expansive geotechnical engineering, cracks result in severe deterioration in the engineering properties of the rock and soil mass and thus can cause serious damage to engineering buildings and structures (Yin et al., 2007). Consequently, scholars have conducted numerous systematic studies on swelling rocks

and soil cracks. Currently, there exist several research results on the crack development characteristics and quantitative description of expansive rock and soil. Lu et al. (2002) and Chen (2014) employed CT technology to study the fracture evolution of expansive soil, which revealed the dynamic process of crack development, new crack connections, and crack formation networks. Yi et al. (1999) studied the fractal characteristics of the fracture structure of expansive soil based on the fractal theory. Wang et al. (2010) proposed a quantitative description method for swelling rock fractures based on the numerical processing technology of image gray and binarisation. Wei et al. (2015) conducted a quantitative analysis of cracks on the surface of expansive soil samples through indoor dry-wet cycle experiments and studied the changes in the geometric structure and morphological characteristics of the crack network according to the number of cycles. Tang et al. (2012) studied the effect of temperature on shrinkage cracks in expansive soil and found that shrinkage cracks exhibit obvious temperature effects. Mao et al. (2018) studied the effects of different initial damage degrees, different numbers of dry and wet cycles, as well as the coupling conditions of these two on the development and evolution of pores and fissures in expansive soils. Their effect on the corresponding soil deformation and mechanical behaviour were examined as well. Moreover, there have been several studies examining the occurrence and propagation mechanism of cracks in swelling rock and soil using experimental, theoretical, and numerical models. Konrad and Ayad (1997) established a theoretical model of clay cracking under the condition of surface evaporation based on the results of field experiments on dry cracking of clay. Further, Yao et al. (2002) proposed a mathematical expression for crack propagation depth using elastic theory and fracture mechanics principles, and determined the approximate depth of crack propagation. Ma et al. (2007) studied the crack generation and propagation process and consequently summarised the crack generation and propagation law. Wu et al. (2011) studied the development mechanism of initial cracks in expansive soil with changes in water content and established a theoretical model. The studies mentioned have mainly focused on the shrinkage cracks of swelling rock and soil under the condition of water loss. However, under the condition of water absorption, expansive soil generally does not produce cracks, whereas expansive rock produces moisture-absorbing expansion cracks. Because the formation mechanism of the swelling rock moisture-absorbing swelling fissures is quite different from the above research results, the above theory cannot be extended to the moisture-absorbing swelling fissures of mudstone without considering the different circumstances. Therefore, research on the quantitative analysis and formation mechanism of hygroscopic swelling cracks is still lacking.

Regarding the disintegration experiments of red-bed mudstone in different acidic or alkaline environments, there exist many research results. Studies have shown that under acidic conditions ($pH < 7$), with an increase in H^+ concentration, the disintegration speeds up, whereas under alkaline conditions, with the increase in OH^- concentration, the disintegration speed slows down. Moreover, the disintegration speed of mudstone varies with mineral composition, soluble cement content, rock texture, grain pattern, porosity, granularity, and degree of weathering (Moon et.al., 1993; Gupta et al., 2007; Yagiz et al., 2010; Ghobadi et al., 2011; Gautam et al., 2013; Fereidoooni et al., 2018;). Critelli et al. (2014) and Yuan et al. (2019) demonstrated that hydrophysical and chemical reactions can result in the generation of secondary pores and changes in mineral composition, which affect the macro-mechanical properties of

sandstones in acidic and alkaline solutions. Zhou et al. (2005) asserted that the role of H + in soft rock softening is related to mineral dissolution. Spagnoli et al. (2012) believed that pH affected clay properties owing to its effect on the particle association of clay minerals. Zhao et al. (2018) explained the effect of pH on the disintegration of purple mudstone from the perspective of the release of K^+, Na^+, Ca^{2+}, and Mg^{2+} cations. However, because the red beds in the southwestern region are very different from those in other regions (grain density, mineral composition, stratum lithology, porosity, weathering degree, etc.), they exist in different acid-base environments and consequently research regarding them is scarce. This is because the mudstone in this area exhibits characteristics such as high particle density, high clay content, strong hydrophilicity, and low resistance to metamorphism. Thus, the above research results cannot be extended to red-bed mudstones in southwestern China.

In this study, a self-designed water absorption device was employed and a CCD camera was used to record the deformation and destruction information of the sample during the water absorption process. Subsequently, the digital speckle correlation method was used to analyse the deformation field. Further, scanning electron microscopy, X-ray diffraction (XRD) experiments, mercury intrusion experiments, and other methods were combined to study the self-absorption cracking characteristics and micro-mechanisms of mudstone in the dry state of the southwestern region in different pH solutions. In addition, real-time monitoring of water absorption and fracture expansion of mudstone, as well as the displacement field and strain field of each point on the upper surface of the sample were realised. Moreover, binarisation was used to obtain the morphology of moisture-absorbing swelling cracks at different moments, and thus, the relationship between water absorption and cracking rate with time was quantitatively analysed. Consequently, three microscopic mechanisms explaining the development of moisture-absorbing swelling fractures in red-bed mudstone and four effects of different pH solutions on the expansion of mudstone fractures were proposed. These complement the current research on the mechanism of moisture absorption and cracking of mudstone and the effect of pH on the microscopic mechanism of mudstone cracking in red beds in central Sichuan. Furthermore, the results of this study is expected to be of significance and aid in roadbed design, tunnel support, slope treatment, and other projects in the southwest region.

2. Experimental And Analytical Methods

2.1. Site description

The samples used in this study were acquired from latitude 29°62' N, longitude 104°73' E, Zizhong County, Neijiang City, Sichuan Province, China. This is a subtropical humid climate zone with a mild climate and abundant rainfall. The highest temperature recorded is 39.9 ℃, and the lowest is -4°C, with the annual average temperature being 17.5°C. The average annual rainfall received by this area is 972.7 mm, with 70% of the rainfall occurring in summer and autumn. The stratum lithology of this area is shown in Fig. 1. The red stratum originated from the Middle Jurassic Xintiangou Formation (geological age mark: J2x).

2.2. Experimental program

Considering the requirements for performing surface crack observation (the thinner the sample, the easier the cracks appear, the easier it is to observe) and the difficulty of sample preparation (the thinner the sample, the more difficult it is to prepare) (2021), the sample was processed into a cylindrical shape (diameter, 80 mm; height, 20 mm). Subsequently, according to the test standard of ISRM (1993), the density, natural water content, and initial porosity of the mudstone samples were measured, as shown in Table 1. Further, to reduce the influence of the difference between samples on the experimental results, five groups of samples (2, 5, 7, 8, and 13) with similar basic properties of mudstone samples were selected under different pH values (3, 5, 7, 9, 11).

Table 1
Basic properties of mudstone samples

Sample number	pH	Density(g/cm^3)	Natural moisture content(%)	Initial porosity(%)
1	/	2.61	3.21	0.7649
2	3	2.55	3.14	0.8436
3	/	2.61	3.42	0.9542
4	/	2.58	3.36	1.0188
5	5	2.56	3.17	0.8221
6	/	2.53	2.95	0.6657
7	7	2.56	3.18	0.8325
8	9	2.59	3.19	0.8171
9	/	2.62	3.16	0.9039
10	/	2.55	3.46	1.0573
11	/	2.62	2.95	0.5708
12	/	2.53	2.95	0.7326
13	11	2.56	3.16	0.8537
14	/	2.59	2.71	0.6554
15	/	2.62	2.95	0.6705

2.3. Sample materials and experimental procedures

The core of the test is dug up at the construction site, wrapped in plastic wrap and sealed in a plastic box. Stay in place by avoiding exposure of rock samples to ambient humidity. The sample was acquired from the same intact rock at a depth of 30 m, and the mineral composition of the mudstone was determined

by XRD analysis. The XRD measurement data acquisition range was 2–65, and the scan rate was 0.02°/2. Mudstone is primarily composed of detrital (quartz, calcite, and hematite) and clay minerals (kaolinite, chlorite, illite, and montmorillonite), and the percentage content of each component is shown in Fig. 2.

The experimental device diagram is shown in Fig. 3, which comprises a CCD camera, precision electronic scale, data acquisition instrument, computer, communication device, and other instruments. The experiment was performed by executing the following procedure: (1) five groups of samples were placed in an oven at 60°C for drying (as shown in Fig. 4(a)). (2) The top surface of the rock sample was coated with the spot marking paint, and again placed in an oven at 60°C for drying to volatilise the moisture in the spot marking paint. Thereafter, small black dots were drawn on the upper surface of the white with black oily strokes to create speckles (as shown in Fig. 4 (b)). (3) Subsequently, the sample was placed on a permeable stone till the display on the electronic scale was stable, and the liquid levels in the two containers were level. The camera position was adjusted to face the sample. During the experiment, the water absorption of mudstone was recorded by recording the display of the electronic scale. (4) The readings of the electronic scale were recorded at regular intervals, and simultaneously, pictures of the upper surface of the rock sample were acquired. Finally, the experiment was ended after the readings on the electronic scale and the crack growth degree on the upper surface of the rock sample stabilised.

The digital speckle correlation method, also referred to as the digital image correlation method, is a non-contact measurement method that records the digital image of the deformation process, and in this study the measurement target was the deformation field of the object. The measurement range was according to the small deformation, vibration, and large deformation of the object, all of which were applicable, with the characteristics of high calculation accuracy and wide measurement range (Song et al., 2011; Mi et al., 2013; Sun et al., 2019). The basic principle of the digital speckle correlation method involves the comparison of the points in the two speckle images. If two points in the correlation window possess the same gray value, they are considered to be the ‘same point’ before and after the deformation. Thus, by comparing the moving distance and moving direction of the point, the surface deformation of the object was calculated. Because of the influence in this study, we mainly focused on the influence of pH on mudstone hygroscopic expansion and displacement field evolution analysis and maximum principal strain evolution analysis.

3. The Influence And Significance Of Ph On Swelling Fractures Of Mudstone

3.1 The influence of pH on the moisture absorption characteristics of mudstone

The change in the water absorption rate of the mudstone sample over time is shown in Fig. 5. It can be concluded that the water absorption of each sample increased with time, and the trend of the water

absorption curve of each sample was fundamentally the same; however, the final water absorption rate was different. The time-history curve of water absorption of mudstone samples exhibited two stages: a rapid growth stage and a slow growth stage. The rapid growth phase was completed within the first 30 min, and the water absorption rate accounted for approximately 90% of the total. In contrast, the duration of the slow growth phase was longer, and the water absorption rate was smaller. The self-absorption process of mudstone is primarily affected by various suction changes, mainly capillary suction and interlayer suction, both of which are collectively referred to as matrix suction (Fan et al., 2002; He et al., 2008). During the early stage of water absorption, the capillary force in the dry mudstone sample was much greater than the interlayer suction, and the water absorption rate increased rapidly with an increase in time. Consequently, the capillary suction in the sample gradually decreased. However, when the capillary suction was equal to the interlayer suction, the growth rate of water absorption decreased. Thereafter, with increase in the water content, the capillary suction and interlayer suction gradually decreased, and finally when the two values decreased to zero, the water absorption rate also became zero and thus, the mudstone water absorption process was complete.

It is evident from the figure that when the pH of the solution is 3, 5, 7, 9, and 11, the final water absorption rates of mudstone are 15.77, 14.58, 13.67, 12.66, and 11.71%, respectively. Therefore, the acidic environment promoted the final water absorption rate of mudstone, whereas the alkaline environment had an inhibitory effect. The main factors affecting mudstone water absorption are the size of mudstone porosity, mineral content and type, and the occurrence of clay minerals. In different acidic or alkaline environments, the clay minerals of the mudstone react with different pH solutions, such as mineral dissolution, ion exchange, and particle association (Su et al., 2002). Consequently, the mineral composition and pore structure of the mudstone change, resulting in a difference in the final water absorption rate of the mudstone under different pH values.

3.2 The influence of pH on the swelling fracture of mudstone

Figure 6 shows the time-varying variation in fracture propagation in mudstone under different pH values. The upper part of each picture is a physical picture acquired via a camera at different times, and the lower part of the picture is a picture that binarises the camera photo at the corresponding time. The surface crack distributions of the mudstone samples at different times were extracted. It is evident from the figure that the fracture expansion of mudstone in the process of self-priming primarily occurred during the rapid growth stage of self-priming. The expansion of the mudstone surface cracks was observed to be stable when the self-priming time was 60 min. However, owing to no restriction on the side, microcracks exist on the side simultaneously when the mudstone sample is self-absorbed. Thus, the water migration rate on the side is faster than that in the middle part, and the side microcracks become the dominant channel for water migration in the self-absorption process. First, the moisture reaches the upper surface of the sample from the side. Simultaneously, owing to the uneven distribution of clay minerals and moisture, expansion stress is generated inside the sample. Because the side surface is unconstrained, compared to other parts of the mudstone sample, it is a weak structural surface, which is

prone to stress concentration. Therefore, the crack generally begins to expand from the side, which upon reaching the upper surface of the sample, results in the formation of a crack along the center of the sample. This crack is a first-order crack developed by a crack on the upper surface.

It can be observed from the Fig. 6 that a single fissure is mostly curved, and the development and expansion of fissures does not expand at a certain angle, which contrasts with homogeneous materials such as metals. Mudstone is an inhomogeneous body, mainly owing to the uneven content and spatial distribution of clay minerals. However, it is evident from the figure that the initiation of child fissures generally develops perpendicular to the main fissures. This is because once the main crack is formed, the deformation restriction perpendicular to the direction of the main crack is released and the corresponding strain energy are released, which causes the strain energy parallel to the development direction of the main crack to continue to accumulate, thereby continually increasing the tensile stress field. However, when the tensile strength of the mudstone is exceeded, a new sub-level crack is formed perpendicular to the direction of the main crack. (Tang et al., 2012; 2018).

The primary geometric parameters of the commonly used cracks are as follows: the number of cracks, average width of the cracks, maximum width of the cracks, and surface crack rate. Because there exist many cracks in this study and their development is complicated, in this experiment the surface crack rate index was employed to quantitatively analyze the evolution process of the expansion cracks (Zhou et al., 2002; Liu et al., 2021). This indicator comprehensively considers the degree of crack development, and the calculation formula is as follows:

$$S_r = \frac{\sum_1^N S_i}{S_0}$$

1

where Sr is the fissure rate and S_i is the area of each crack. Further, assuming that there are N cracks in the sample, S_0 is the initial area of the upper surface of the sample.

It is evident from Fig. 7 that the trend of the change curve of the mudstone fissure rate with time under different pH values is similar. The initiation time of mudstone samples increased with an increase in pH value. Further, the graph of fissure rate exhibits a change with time, which can be roughly divided into two stages: the rapid development stage and the stable stage. At pH values of 3, 5, 7, 9, and 11, the final fracture rates of mudstone are 18.909, 14.139, 12.341, 11.856, and 7.111%, respectively. The above results indicate that the increase in H^+ concentration results in an increase in the development of moisture-absorbing fissures in mudstone, and vice-versa. Moreover, considering the binarisation diagram of the mudstone sample that in an acidic environment, it is evident that there are more and denser fractures in the mudstone sample than in an alkaline environment, and the development of the fracture network is more complicated. Thus, this shows that the current increase in acid rain pollution in

southwestern China may aggravate the expansion of red bed mudstone fissures in this area and increase the risk of engineering disasters such as subgrade arching and slope instability.

4. Analysis Of The Effect Of Ph On The Evolution Of Swelling Deformation Of Mudstone

4.1 Influence of pH on swelling of mudstone and evolution of displacement field

During the entire mudstone moisture absorption expansion and cracking process, the mudstone moisture absorption expansion deformation and displacement change diagrams at different times were obtained, as shown in Fig. 8. It is evident that the combined displacement on the outside of the specimen is greater than that on the inside. However, when the combined displacement changes from the outside to the inside of the diameter, an irregular decreasing form of concentric circles is observed rather than a regular decreasing form. This confirms the differences in the combined displacement of mudstone on the same radius circle. With an increase in the moisture absorption and expansion time of mudstone, the combined displacement of mudstone expansion gradually increased from the outside to the inside, and the moisture absorption and expansion of mudstone exhibited differential expansion. In addition, the fracture network was employed to divide the entire area into several small areas, and the combined displacement value of the outer area was greater than that of the internal measurement area. Moreover, because of the existence of a deformation space in the outer area, it is more conducive to the generation and expansion of cracks.

Simultaneously, under different pH values, the maximum total displacement value of mudstone swelling due to moisture absorption decreased with increasing pH value, thereby demonstrating that an acidic environment promotes moisture swelling and deformation of mudstone. Moreover, as the pH value decreased, the mudstone speckle interference fringes became more turbulent and the fluctuation amplitude increased, which indicated that under an acidic environment, the moisture absorption and expansion of the mudstone surface produced more cracks, thereby resulting in the disappearance of certain scattered spots and discontinuity of displacement on both sides of the cracks. Therefore, there were more sudden changes in the combined displacement cloud image. Further, as the pH value increased, the absolute value of the combined displacement on both sides of the fracture decreased. This is because of the uneven distribution of mudstone clay minerals and the uneven spatial distribution of water during mudstone self-absorption. When clay minerals encounter acidic solutions, they produce a greater swelling force and thus, the differential expansion of mudstone is more obvious.

4.2 The influence of pH on the evolution analysis of the maximum principal strain of mudstone hygroscopic swelling

During the entire process of mudstone swelling, the maximum principal strain cloud diagrams at different moments of mudstone swelling were obtained, as shown in Fig. 9. It is evident that the maximum

principal strain around the fissure is larger than that of other uncracked parts, which is consistent with the mechanism by which the moisture-absorbing swelling fissure of mudstone generates and expands along the maximum principal strain (maximum principal stress). Simultaneously, in the process of moisture absorption and expansion of mudstone, the maximum principal strain does not develop in a certain direction in contrast to a homogeneous material, and shows irregularity. This shows that mudstone is not a homogeneous body, its clay minerals are unevenly distributed in space, and that it absorbs water unevenly. Further, the fissure divides the mudstone surface area into several expansion strain zones. Moreover, in contrast to homogeneous materials, there is only one expansion core, but each strain zone has one expansion core. Further, for each expansion strain zone divided by the cracks, the surrounding cracks provide a space for deformation, and the maximum principal strain measured outside the expansion strain zone was greater than that measured inside. Consequently, when the maximum principal strain at a certain point outside the expansion strain zone underwent a sudden change, the crack further divided the expansion strain zone along this weak point to obtain more expansion strain zones.

Under different pH values, with an increase in the pH value, the maximum principal strain value of the mudstone swelling deformation simultaneously decreased, which indicated that the acidic environment was more conducive to moisture absorption and cracking of mudstone than an alkaline environment. Moreover, following the completion of the swelling of mudstone, more swelling strain zones were observed in the acidic environment than in the alkaline environment, and the difference in the maximum principal strain value between adjacent strain zones was greater. This shows that mudstone forms greater number of fissures, and the degree of rock mass fragmentation is greater in an acidic environment.

5. Discussion On The Micro-mechanism Of Ph Influence

5.1 Three micro-mechanisms of hygroscopic fissure propagation in red mudstone

The crack propagation mechanism of red mudstone primarily includes hydration-swelling and softening, adsorption-wedge failure, and humidity stress field. Hydration-swelling and softening are chemical processes of hydration, expansion, and exfoliation of clay minerals. Clay minerals in red mudstone, such as hydrophilic montmorillonite, easily absorb water, resulting in the formation and expansion of the hydration of the electric double layer (Chenevert et al.,1970; Fairhurst et al.,2002). The clay particles then increase in size owing to crystal expansion and osmotic expansion (Miller et al., 1990; Fukue et al., 1999). Consequently, the resulting expansion pressure reduces the attractive force between the structural connections and the bonds between the particles are broken, leading to the development of mudstone cracks.

Adsorption-wedge failure (Fig. 10) is a mechanical process involving crack initiation, propagation, and coalescence (Terzaghi et al., 1967). Mudstone absorbs water under the action of matric suction.

Simultaneously, cracks and pores are conducive to water absorption and are the dominant channels for water migration, resulting in increased capillary pressure and gas pressure. In addition, both pressures tend to promote crack propagation and coalescence (Liu et al., 2020). Consequently, the bond between carbonate and clay minerals is broken by the two pressures, which causes the red mudstone to crack. Thus, water enters the pores and fissures and results in the formation of a strength damage zone with the contacted matrix (Fig. 10), which causes stress concentration at the junction of the strength damage zone and the intact bedrock. Subsequently, under the interaction of capillary pressure and gas pressure, the stress concentration area promotes the generation and propagation of cracks.

The theory of the humidity stress field was proposed by Professor Miao Xiexing (1993; 1995), who highlighted that the diffusion of water in a swelling rock mass is coupled with water content, water absorption, volume deformation, etc. The red-bed mudstone in central Sichuan is a heterogeneous body composed of different minerals. Thus, the expansion coefficients of various minerals are different under the influence of the humidity field, such that the deformation of various mineral particles is different after mudstone encounters water. as mudstone is a continuum, to ensure the continuity of deformation, various mineral particles in the mudstone cannot freely deform according to their inherent expansion coefficient with the change in humidity. Therefore, there exist mutual constraints among clay mineral particles, and those with large deformations are compressed, while those with small deformations are stretched. Consequently, a type of humidity structural stress was formed in the mudstone. Moreover, maximum stress often occurs at the junction of the mineral particles, which upon reaching or exceeding the tensile strength of mudstone, results in the connection between the mineral particles being broken, thereby resulting in cracks (Ji et al., 2009; Xu et al., 2018).

When mudstone is self-absorbed, hydration expansion and softening reduce the strength of the mudstone itself, thereby rendering it easier for adsorption-wedge pressure and humidity stress to break the bond between mudstone particles and form cracks. Consequently, the appearance of cracks provides an advantageous channel for the migration of water and enhances the adsorption-wedge failure of mudstone and the humidity stress field effect. Moreover, in the process of mudstone self-absorption, the three mechanisms complement each other and work together to accelerate the fracture of the connection between mudstone particles, as well as the generation, expansion, and penetration of cracks.

5.2 Four influences of pH value on the propagation of mudstone fissures

The influence of acidic and alkaline solutions on the fracture expansion of red-bed mudstone primarily includes the following four aspects: mineral dissolution, ion absorption and exchange, particle association, and pore changes. The dissolution of minerals affects the chemical decomposition process of the red-bed mudstone in central Sichuan, which mainly manifests as dissolution and erosion. The dissolution equation of mudstone clay minerals in an acid-base environment is shown in Table 2. As shown in Table 2, clay minerals are more soluble in acidic environments, illite and montmorillonite are dissolved and transformed into kaolinite in an acidic environment, and mudstone contains kaolinite.

Therefore, in acidic environments, the kaolinite content in mudstone is significantly greater than that in neutral and alkaline environments. Further, kaolinite exhibits high hygroscopicity, thereby promoting hydration swelling and softening (Yong et al., 1979), which causes the final water absorption rate of mudstone in acidic environments to be higher than that in neutral and alkaline environments. In addition, H^+ dissolves haematite and breaks the carbonate cementation in calcite (Zhang et al., 2018), which promotes the generation, expansion, and penetration of cracks in acidic environments.

Table 2
Dissolution reaction equation of red-bed mudstone clay minerals (Li et al., 2016; Feng et al., 2010; Yuan et al., 2019)

solutions	minerals	chemical reaction equations
acid	Quartz	$SiO_2 + 2H_2O = H_4SiO_4$
	Albite	$NaAlSi_3O_8 + 4H^+ + 4H_2O = Na^+ + Al^{3+} + 3H_4SiO_4$
	Calcite	$CaCO_3 + 2^{H+} = Ca^{2+} + H_2O + CO_2$
	Hematite	$Fe_2O_3 + 6H^+ = 2Fe^{3+} + 3H_2O$
	Montonorillonite	$Na_x(H_2O)_4\{(Al_{2-x}Mg_x)[Si_4O_{10}](OH)_2\} + H_2O + H^+ \rightarrow Na^+ + Mg^{2+} + Al_2O_3(2SiO_2)(2H_2O) + H_4SiO_4$
	Illite	$K\{Al_2[AlSi_3O_{10}](OH)_2\} + H_2O + H^+ \rightarrow Al_2O_3(2SiO_2)(2H_2O) + K^+$
Neutral	Quartz	$SiO_2 + 2H_2O = H_4SiO_4$
	Calcite	$CaCO_3 = Ca^{2+} + CO_3^{2-}$
	Albite	$NaAlSi_3O_8 + 5.5H_2O = 0.5Al_2Si_2O_5(OH)_4 + K^+ + OH^- + 2H_4SiO_4$
Alkaline	Quartz	$SiO_2 + 2OH^- = H_2SiO_4^{2-}$
	Albite	$NaAlSi_3O_8 + 6OH^- + 2H_2O = Na + + Al(OH)^-_4 + 3H_2SiO_4^{2-}$
	Calcite	$CaCO_3 = Ca^{2+} + CO_3^{2-}$

Ion exchange is an exchange process between ions and molecules adsorbed to mineral particles via physical and chemical forces and water (Kozaki et al., 2005). Owing to the large specific surface area of clay minerals, a large amount of colloidal substances are adsorbed on the surface, and ion exchange with ions in water is easier. Further, when mudstone is self-absorbed in an acidic solution, H^+ can be replaced by cations such as K^+, Al^{3+}, Ca^{2+}, and Mg^{2+}, which may cause the crystal lattice to separate from the water phase, which results in the dissolution of montmorillonite (Townsend et al., 1984). In addition, in the acidic environment of mudstone, bond breaks are usually formed on the edges or non-cleavage

surfaces of clay mineral particles in contact with water after the minerals are dissolved, and bond breaks increase with a decrease in clay minerals. As both sides of the broken bond are charged positively and negatively, this effect promotes the ion exchange capacity. Consequently, the ion exchange adsorption results in the transformation of minerals in the mudstone self-absorption process, and thus the cementation between particles is destroyed, thereby promoting the formation of mudstone fissures.

The association of particles affects the chemical decomposition of clay minerals in the mudstone of the central Sichuan red bed when it comes in contact with water, thereby affecting the generation, expansion, and penetration of moisture-absorbing fissures in the mudstone. In addition, the combination of the two particles reflects the dominant interparticle force. There exist three common types of minimum energy particle flocculation: edge-to-face, edge-to-edge, and face-to-face (Olphen et al., 1977). When H^+ and OH^- concentrations are increased various charges are generated on the exposed edges of mineral particles, resulting in a gradual increase in positive or negative charges on the outer surface of the particles. Therefore, when the diffusing double layer and the force between the particles change, the charges between the particles form different combinations (Santamarina et al., 2002). Under acidic conditions, the Coulomb force between the positive and negative sides results in flocculation between the sides of the particles. However, this flocculation state is unstable, the structure is loose, and there exist sufficient space between the particles, which is good for adsorbing more water and promoting the moisture absorption of mudstone. In an alkaline environment, negatively charged particles form face-to-face flocculation through osmotic repulsion and van der Waals forces, and the structure formed is relatively stable, with the particles being closely arranged. However, this is not conducive to water adsorption. Under neutral conditions, owing to the decrease in the Coulomb repulsive force from edge to edge and the repulsive force from face to face, edge to edge flocculation can be observed. In addition, the stability of this state is between that of the previous two (Vanolphen et al 1951).

Pore changes cause a change in the water migration rate of the red-bed mudstone, thereby affecting the rate of crack expansion in the red-bed mudstone. The pore size classification in coal is based on the Hodot pore classification method (Li et al 2015), and are classified as follows: micropores ($D < 10$ nm), transition pores ($10 \leq D < 100$ nm), mesopores ($100 \leq D < 1\,000$ nm), and macropores ($\geq 1\,000$ nm). Figure 12, 14, 16, and 13, 15, and 17 show the pore size-pore volume distribution and pore size-specific surface area distribution of mudstone under different pH conditions, respectively. The pore structure and pore size of mudstone are shown in Figure (Wang et al 2021). Combined with Table 3, it is evident that when pH = 3, the mudstone pore size-pore volume distribution curve has a peak when the pore size is 17.11 nm. Moreover, micropores and transitional pores contributed more to the total pore volume, with the values being 0.0942 and 0.1620 $mL \cdot g^{-1}$, respectively, at a contribution rate of 46.29%. Simultaneously, the specific surface area curve of mudstone has a single peak at a pore size of 6.48 nm, where the micropores and transition pores contributed the most to the total surface area, with surface area values of 18.5659 and 9.3206 $m^2 \cdot g^{-1}$, respectively, at a contribution rate of 99.7%. Further, when pH = 7, the mudstone pore size-pore volume distribution curve has a peak when the pore size is 17.11 nm, with micropores and transitional pores contributing more to the total pore volume having values of 0.1 and

0.1678 $mL \cdot g^{-1}$, respectively, and a contribution rate of 60.37%. Moreover, the mudstone specific surface area curve has a single peak at a pore size of 13.73 nm, wherein micropores and transition pores contributed the most to the total surface area, with specific surface area values of 19.9116 and 11.6297 $m^2 \cdot g^{-1}$, respectively, at a contribution rate of 99.76%. Furthermore, when pH = 11, the mudstone pore size-pore volume distribution curve has a peak when the pore size is 17.11 nm. Herein, the micropores and transitional pores contributed more to the total pore volume, with values of 0.1163 and 0.2222 $mL \cdot g^{-1}$, and the contribution rate reached 61.88%. Simultaneously, the specific surface area curve of mudstone has a single peak at 6.03 nm pore size, with the micropores and transition pores contributing the most to the total surface area, with values of 20.9757 and 12.6972 $m^2 \cdot g^{-1}$, respectively, at a contribution rate of 99.71%. Thus, the analysis showed that with an increase in the pH value, the pore volume and the proportion of the pore volume of the micropores and transition pores in the mudstone gradually increased, which indicates that the acidic environment promotes the transformation of mudstone micropores and transitional pores into mesopores and macropores. Therefore, an acidic environment is conducive to the generation, expansion, and penetration of mudstone water and moisture absorption fissures.

Table 3
Distribution results of pore size-pore volume/specific surface area of mercury intrusion experiments under different pH conditions

	Pore size d(nm)	d < 10	100 > d > 10	1000 > d > 100	100000 > d > 1000	d > 100000	dHg (Full pore size)
PH = 3	Pore volume(10^{-4}mL/g)	0.0942	0.1620	0.1620	0.1268	0.0084	0.5534
	Pore volume ratio(%)	17.020	29.267	29.267	22.921	1.525	100
	Specific surface area($10^{-4}m^2/g$)	18.5659	9.3206	0.0667	0.0173	0.0001	27.9706
	Ratio of specific surface area(%)	66.37655	33.32290	0.23834	0.06171	0.00051	100
PH = 7	Pore volume(10^{-4}mL/g)	0.1000	0.1678	0.0534	0.1143	0.0081	0.4436
	Pore volume ratio(%)	22.540	37.826	12.042	25.777	1.815	100
	Specific surface area($10^{-4}m^2/g$)	19.9116	11.6297	0.0627	0.0134	0.0001	31.6175
	Ratio of specific surface area(%)	62.97652	36.78254	0.19829	0.04223	0.00042	100
PH = 11	Pore volume(10^{-4}mL/g)	0.1163	0.2222	0.0944	0.1069	0.0072	0.5471
	Pore volume ratio(%)	21.257	40.622	17.257	19.541	1.323	100
	Specific surface area($10^{-4}m^2/g$)	20.9757	12.6972	0.0856	0.0112	0.0001	33.7698
	Ratio of specific surface area(%)	62.11384	37.59916	0.25351	0.03313	0.00036	100

Thus, the four processes of mineral dissolution, ion absorption and exchange, particle association, and pore change synergistically affect the chemical decomposition and physical decomposition of the red mudstone in central Sichuan through hydration, expansion, dissolution, expansion, and exfoliation. This results in three distinct mechanisms in different pH solutions having different effects. Therefore, the final moisture absorption rate and final fracture rate of mudstone at different pH values are quite different.

6. Conclusion

Through the self-absorption experimental device designed for the study, real-time monitoring of mudstone water absorption and fracture rate under different pH values was realised. Thereafter, the digital speckle correlation method was used to analyse the deformation and evolution of mudstone in different pH solutions. Further, by combining scanning electron microscopy and mercury intrusion experiments, we analysed the microscopic changes of mudstone under different pH solutions. Thus, this experiment studied the moisture absorption and cracking characteristics of red mudstone in different pH solutions and their micro-mechanisms, and the main conclusions drawn are as follows:

(1) The acidic environment was found to promote the self-absorption of red-bed mudstone, whereas an alkaline environment inhibited it. When the pH value of the solution was 3, the final water absorption rate of the red-bed mudstone was the highest (15.77%), whereas it was lowest at solution pH value of 11 (11.71%).

(2) Red-bed mudstone experiences moisture-absorbing swelling cracks in different pH solutions, and the rate of crack development is mainly concentrated in the rapid water absorption stage. As the pH increased, the final fracture rate of the red mudstone decreased. For solution pH value of 3, the final fracture rate of the red mudstone was the highest (18.909%), whereas it was lowest when the solution pH was 11 (7.111%).

(3) The combined displacement field and maximum principal strain of the self-priming deformation and evolution of mudstone in different pH solutions were analysed, and it was concluded that mudstone exhibits differential expansion. The maximum combined displacement and maximum principal strain of mudstone in an acidic environment weas larger than those in an alkaline environment. Moreover, with decrease in the pH value, the speckle interference fringe cloud image of the swelling of mudstone became more turbulent and fluctuated. Simultaneously, the failure characteristics of the mudstone exhibited increased swelling strain areas and swelling cores.

(4) This study clarified the microscopic mechanism of swelling fractures in mudstone under different pH solutions. Specifically, the moisture-absorbing swelling fractures of red-bed mudstone were explained via three microscopic mechanisms: hydration-swelling and softening, adsorption-wedge failure, and humidity stress field. Further, solutions with different pH values were found to affect these three microscopic mechanisms through four physical/chemical processes: mineral dissolution, ion absorption and exchange, particle association, and pore changes.

Declarations

Acknowledgments

This research was supported by the National Natural Science Foundation of China (No. 42172308).

Data availability

The experimental data used in our research may be available from the corresponding author by request.

Conflict of interest

The authors declare that they have no competing interests.

References

1. Antamarina JC, Klein KA, Palomino A, Guimaraes MS (2002) In: Maio (ed) Micro-scale aspects of chemical-mechanical coupling. Interparticle forces and fabric. C.D
2. Chenevert ME (1970) Shale alteration by water adsorption. J Petrol Technol 22(9):1141–1148. https://doi.org/10.2118/2401-PA
3. Critelli T, Marini L, Schott J, Mavromatis V, Apollaro C, Rinder T, De Rosa R, Oelkers EH (2014) Dissolution rates of actinolite and chlorite from a whole-rock experimental study of metabasalt dissolution from 2 < = pH < = 12 at 25 degrees C. Chem Geol 390:100–108. https://doi.org/10.1016/j.chemgeo.2014.10.013
4. Chen WW, Yuan PB, Liu XW (2009) Study on creep properties of red-bed soft rock under step load. Chin J Rock Mechan Eng 28(S1):3076–3081
5. Chen ZH (2014) On basic theories of unsaturated soils and special soils. Chin J Geotech Eng 36(2):201–272
6. Dai ZJ, Guo JH, Zhou Z, Chen SX, Yu F, Li J (2020) Inversion and prediction of long-term uplift deformation of high-speed railway subgrade in central Sichuan red-bed. Chin J Rock Mechan Eng 39(S2):3538–3548. https://doi.org/10.13722/j.cnki.jrme.2019.1149
7. Fairhurst CE, H JA (1999) International society for rock mechanics commission on testing methods. Int J Rock Mech Min 36:279–289
8. Fereidooni D, Khajevand R (2018) Determining the Geotechnical Characteristics of Some Sedimentary Rocks from Iran with an Emphasis on the Correlations between Physical, Index, and Mechanical Properties. Geotech Test J 41(3):555–573. https://doi.org/10.1520/GTJ20170058
9. Fredlund DG, Hendry R (1993) Soil mechanics for unsaturated soils[M] [S. l.], John Wiley and Sons: 64–66
10. Fukue M, Minato T, Horibe H, Taya N (1999) The micro-structures of clay given by resistivity measurements. Eng Geol 54(1–2):43–53. https://doi.org/10.1016/S0013-7952(99)00060-5
11. Feng X, Ding W, Cui Q (2010) Coupled chemical-stress effect on rock fracturing process. Science Press, Beijing. (in Chinese)
12. Fan YQ, Liang X, Han JS (2020) Experimental study on saturation and swelling-shrinkage characteristics of unsaturated expansive rocks. Chin J Rock Mechan Eng 39(01):45–56. https://doi.org/10.13722/j.cnki.jrme.2019.0579

13. Ghobadi MH, Momeni AA (2011) Assessment of granitic rocks degradability susceptive to acid solutions in urban area. Environ Earth Sci 64(3):753–760. https://doi.org/10.1007/s12665-010-0895-6
14. Gautam TP, Shakoor A (2013) Slaking behavior of clay-bearing rocks during a one-year exposure to natural climatic conditions. Eng Geol 166:17–25. https://doi.org/10.1016/j.enggeo.2013.08.003
15. Gupta V, Ahmed I (2007) The effect of pH of water and mineralogical properties on the slake durability (degradability) of different rocks from the Lesser Himalaya, India. Eng Geol 95(3–4):79–87. https://doi.org/10.1016/j.enggeo.2007.09.004
16. Guo YC, Xie Q, Wen JQ (2007) Red beds distribution and engineering geological problem in China. Hydrogeol Eng Geol 6:67–71
17. He MC, Zhou L, Li DJ, Wang CG, Lie W (2008) Experimental research on hydrophilic characteristics of mudstone in deep well. Chin J Rock Mech Eng 27(6):1113–1120 (in Chinese)
18. Huang SB, Cheng Q, Hu HT (2005) A study on distribution of Sichuan red beds and engineering environment characteristics.Highway(5):81–85. (in Chinese)
19. Kozaki T, Fujishima A, Saito N, Sato S, Ohashi H (2005) Effects of dry density and exchangeable cations on the diffusion process of sodium ions in compacted montmorillonite. Eng Geol 81(3):246–254. https://doi.org/10.1016/j.enggeo.2005.06.010
20. Konrad JM, Ayad R (1997) Desiccation of a sensitive clay: field experimental observations. Can Geotech J 34(6):929–942. https://doi.org/10.1139/t97-063
21. Ji M (2009) Study on mechanical properties evolution and creep characteristics of calay-mudstone under humidity field. China University of Mining and Technology
22. Liu JD, Tang CS, Zeng H, Shi B (2021) Evolution of desiccation cracking behavior of clays under drying-wetting cycles. Rock and Soil Mechanics 42(10):2763–2772. https://doi.org/10.16285/j.rsm.2021.0459
23. Li L, Tang DZ, Xu H, Meng YJ, Fang N, Tang SL (2015) Pore and fissure structure characteristics of medium rank coal under the control of coal petrology: taking Liulin mining area as the example. China Sci paper 10(9):1058–1065
24. Lu ZH, Chen ZH, Pu YB (2002) A CT study on the crake evolution of expansive soil during drying and wetting cycles. Rock and Soil Mechanics 23(4):417–422 (in Chinese)
25. Liu XM, Song YF, Xia Z, Chen RP (2020) Assessing the slake durability of red stratum sandstone in different solution environments by a novel dual rotation test. Eng Geol 2678. https://doi.org/10.1016/j.enggeo.2020.105503
26. Li XN (2016) Macro and meso damage characteristics of silty mudstone under acidic environment. Southwest Jiaotong University
27. Mi H (2013) Rock mechanical behaviors testing by digital speckle correlation method. J Appl Opt 34(1):123–127. https://doi.org/10.5768/JAO201334.0103006

28. Ma J, Chen SX, Yu F, Feng MG (2007) Experimental research on crack evolution process in fissured clay. Rock and Soil Mechanics 28(10):2203–2208. https://doi.org/10.16285/j.rsm.2007.10.021
29. Miller SE, Low PF (1990) Characterization of the electrical double-layer of montmorillonite. Langmuir 6(3):572–578. https://doi.org/10.1021/la00093a010
30. Moon VG (1993) Geotechnical characteristics of ignimbrite - a soft pyroclastic-rock type. Eng Geol 35(1–2):33–48. https://doi.org/10.1016/0013-7952(93)90068-N
31. Miu XX (1995) Coupling equations of humidity stress field theory.Mechanics in Engineering(6):22–24
32. Miu XX, Yang CY, Chen ZD (1993) Theory of humidity stress field in expansive rock mass. Rock and Soil Mechanics 14(4):49–55. https://doi.org/10.16285/j.rsm.1993.04.009
33. Mao X, Xin SJ, Cheng MS, Chen ZH, Wang XQ (2018) Mechanical behavior of expansive soil under initial damage and wetting-drying cycles. Rock and Soil Mechanics 39(2):571–579. https://doi.org/10.16285/j.rsm.2017.1136
34. Olphen v (1977) Clay Colloid Chemistry, Second Edition. Krieger Publishing Company, Malabar, Florida 318p
35. Spagnoli G, Rubinos D, Stanjek H, Fernandez-Steeger T, Feinendegen M, Azzam R (2012) Undrained shear strength of clays as modified by pH variations. Bull Eng Geol Environ 71(1):135–148. https://doi.org/10.1007/s10064-011-0372-9
36. Sun Q, Cai C, Zhang SK, Tian S, Li B, Xia YJ, Sun QW (2019) Study of localized deformation in geopolymer cemented coal gangue-fly ash backfill based on the digital speckle correlation method. Constr Build Mater 215:321–331. https://doi.org/10.1016/j.conbuildmat.2019.04.208
37. Su XX, Tang HM, Huang L, Shen PW, Xia D (2020) The role of pH in red-stratum mudstone disintegration in the Three Gorges reservoir area, China, and the associated micromechanisms. Eng Geol 279:5873–5873. https://doi.org/10.1016/j.enggeo.2020.105873
38. Song YM, Ma SP, Yang XB, Wang X (2011) Experimental investigation on failure of rock by digital speckle correlation method. Chin J Rock Mech Eng 30(01):170–175
39. Tang CS, Cui YJ, Tang AM, Shi B (2012) Shrinkage and desiccation cracking process of expansive soil and its temperature-dependent behaviour. Chin J Geo-technical Eng 4(12):2181–2187 (in Chinese)
40. Tang CS, Shi B, Cui YJ (2018) Behaviors and mechanisms of desiccation cracking of soils. Chin J Geotech Eng 40(8):1415–1423. https://doi.org/10.11779/CJGE201808006
41. Tang CS, Shi B, Cui YJ, Liu C, Gu K (2012) Desiccation cracking behavior of polypropylene fiber-reinforced clayey soil. Can Geotech J 49(9):1088–1101. https://doi.org/10.1139/T2012-067
42. Terzaghi K, Peck RB (1967) Soil Mechanics in Engineering Practice, seconded. John Wiley & Sons, Inc., New York, NY
43. Townsend RP (1984) Thermodynamics of ion exchang in clays. Philosophical Trans Royal Soc Math Phys Sci 311:301–314. https://doi.org/10.1098/rsta.1984.0030

44. Vanolphen H (1951) Rheological phenomena of clay sols in connection with the charge distribution on the micelles. Discuss Faraday Soc 1182–84. https://doi.org/10.1039/DF9511100082
45. Wei BX, Liu B, Liu X (2015) Research on the quantitative basic index of expansive soil cracks. Hydrogeol Eng Geol 42(5):84–89. https://doi.org/10.16030/j.cnki.issn.1000-3665.2015.05.14
46. Wang J, Gong BW, Zhang JJ, Zhou XW, Tan FY (2010) Field observation and description method of cracks development on expansive rock. J Yangtze River Sci Res Inst 27(9):74–75
47. Wu JH, Yuan JP, Ng CWW (2012) Theoretical and experimental study of initial cracking mechanism of an expansive soil due to moisture-change. J Cent South Univ 19(5):1437–1446. https://doi.org/10.1007/s11771-012-1160-9
48. Wang L, Liu HQ, Xie GX, Yuan QP, Chen LP (2021) Detailed characterization of the pore and fracture structure and strength degradation mechanism of gas-containing coal. Rock and Soil Mechanics 42(12):1–15. https://doi.org/10.16285/j.rsm.2021.1039
49. Xu XL (2018) Study on mechanical properties evolution and microscopic mechanism of granites under temperature loading. China University of Mining and Technology
50. Yao HL, Zheng SH, Ge XR, Yi SX (2002) Assessment on slope stability in cracking expansive soils. Chin J Rock Mechan Eng 21(S2):2331–2335
51. Yong RN, Sethi AJ, Booy E, Dascal O (1979) Basic characterization and effect of some chemicals on a clay from outardes 2. Eng Geol 14(2–3):83–107. https://doi.org/10.1016/0013-7952(79)90079-6
52. Yagiz S (2010) Geomechanical properties of construction stones quarried in South-western Turkey. Sci Res Essays 5(8):750–757. https://doi.org/10.5897/SRE.9000526
53. Yi SM, Li ZH, Zhang YZ (1999) The fractal characteristics of fractures in expansion soil and its significance. Chin J Geotech Eng 3:294–298 (in Chinese)
54. Yuan W, Liu XR, Fu Y (2019) Chemical thermodynamics and chemical kinetics analysis of sandstone dissolution under the action of dry-wet cycles in acid and alkaline environments. Bull Eng Geol Environ 78(2):793–801. https://doi.org/10.1007/s10064-017-1162-9
55. Yuan W, Liu XR, Fu Y (2019) Chemical thermodynamics and chemical kinetics analysis of sandstone dissolution under the action of dry-wet cycles in acid and alkaline environments. Bull Eng Geol Environ 78(2):793–801. https://doi.org/10.1007/s10064-017-1162-9
56. Yang ZC, Zhang JY, Zhou DP (2006) Study on rapid weathering characteristics of red mudstone slope. Chin J Rock Mechan Eng 25(2):275–283
57. Yin ZZ, Yuan JP, Wei J, Cao XS, Liu HQ, Xu B (2012) Influences offissures on slope stability of expansive soil. Chin J Geotech Eng 34(12):2155–2161
58. Zhou CY, Tan XS, Deng YM, Zhang LM, Wang JH (2005) Research on softening micro-mechanism of special soft rocks. Chin J Rock Mech Eng 24(3):394–400
59. Zhong ZB, Li AH, Deng RG, Wu PP, Xu J (2019) Experimental study on the time-dependent swelling characteristics of red-bed mudstone in Central Sichuan. Chin J Rock Mech Eng 38(1):76–86. https://doi.org/10.13722/j.cnki.jrme.2018.0861

60. Zhou Z, Chen SX, Wang YH, Dai ZJ (2021) Crack Evolution Characteristics and Cracking Mechanism of Red Beds in Central Sichuan during Seepage and Swelling. Geofluids 2021:81046–81046. https://doi.org/10.1155/2021/9981046
61. Zhao JX, Lu CH, Deng LM, Liu GC (2018) Impacts of simulated acid solution on the disintegration and cation release of purple rock (mudstone) in Southwest China. Geomorphology 316:35–43. https://doi.org/10.1016/j.geomorph.2018.05.009
62. Zhang Y, Hu ZQ, Li L, Xue ZJ (2018) Improving the structure and mechanical properties of loess by acid solutions - An experimental study. Eng Geol 244:132–145. https://doi.org/10.1016/j.enggeo.2018.07.023

Figures

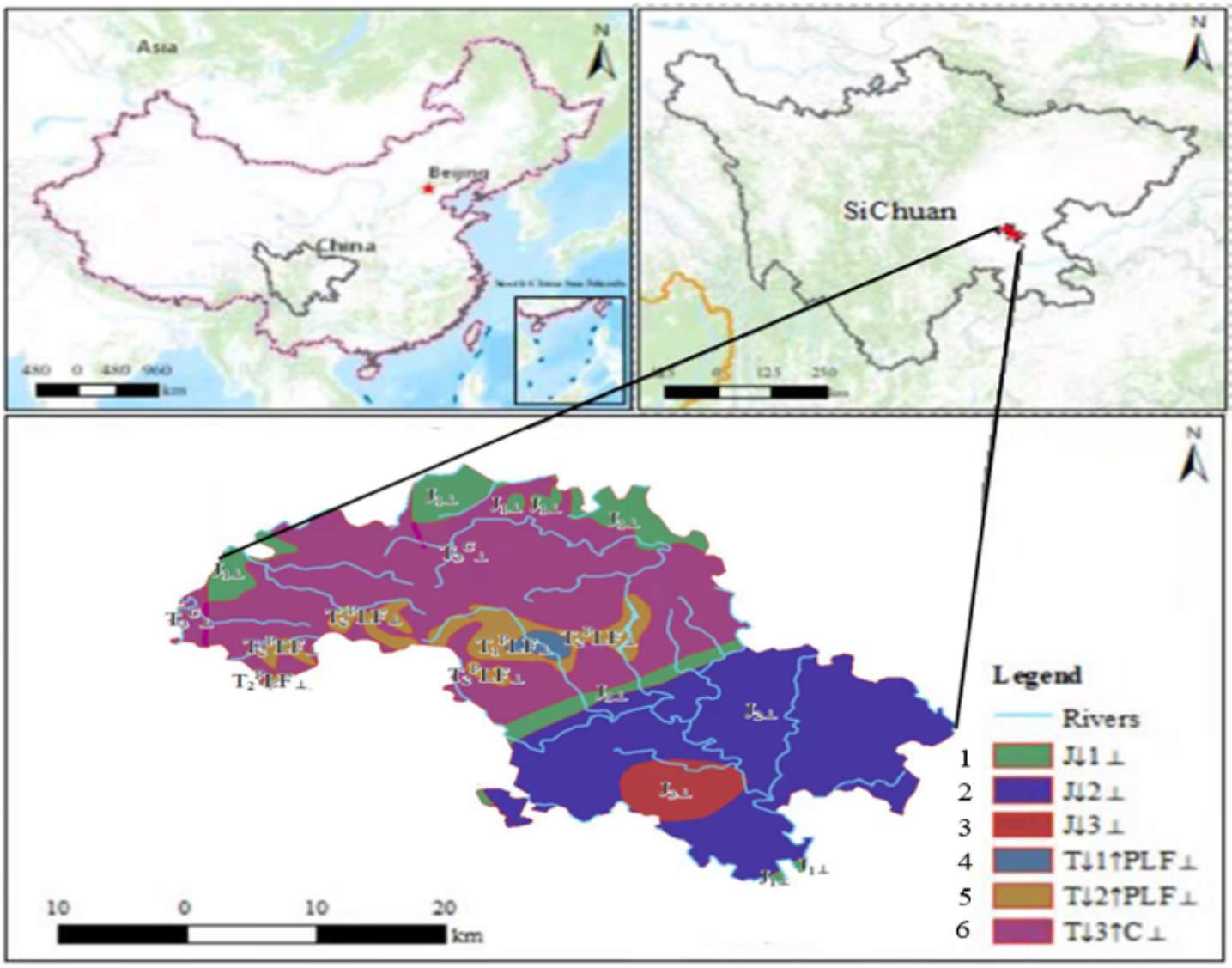

Figure 1

Sampling location：1：Lower Jurassic；2：Middle Jurassic；3：Upper Jurassic；4： Lower Triassic platform facies；5：Middle Triassic platform facies；6：Upper Triassic of continental facies；

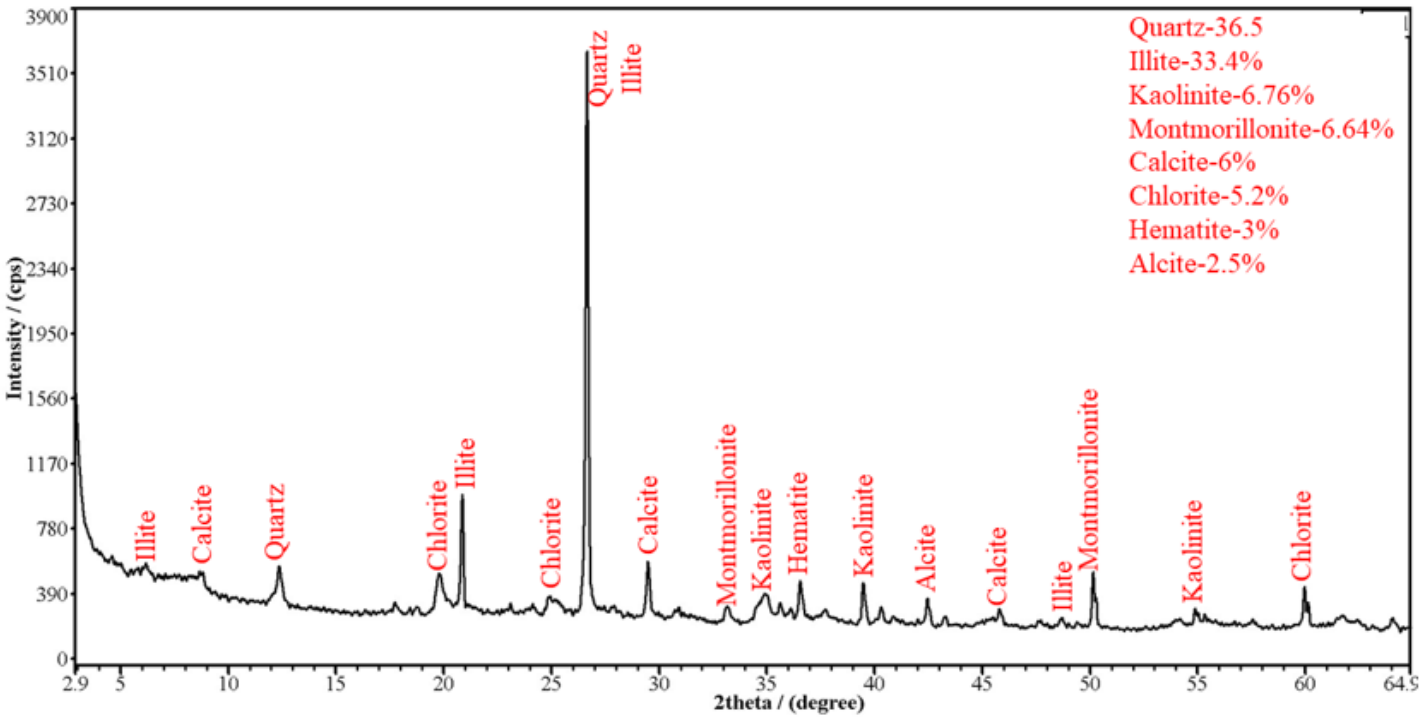

Figure 2

Mineral composition of mudstone samples

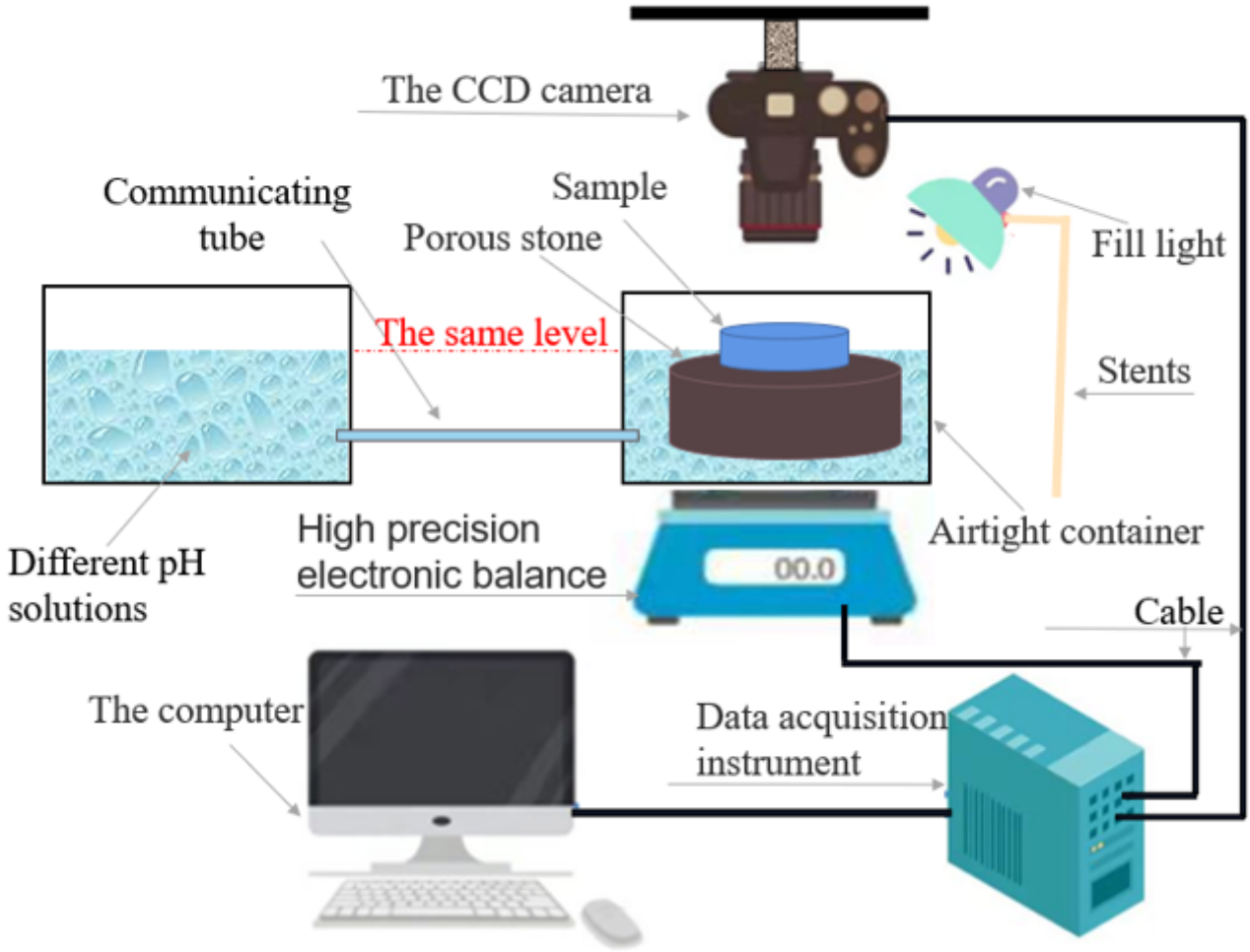

Figure 3

Diagram of experimental setup

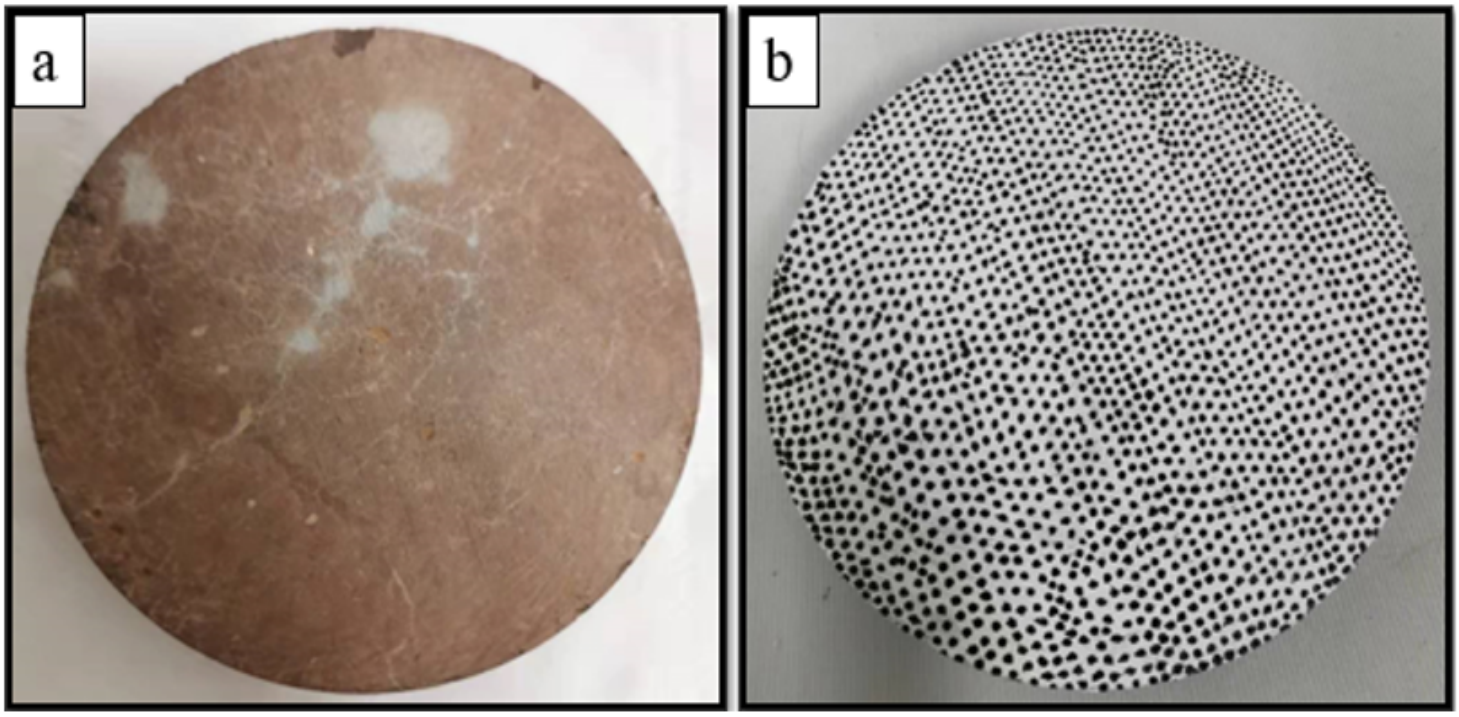

Figure 4

Mudstone sample ((a) mudstone sample after drying, (b) mudstone sample after plaque preparation)

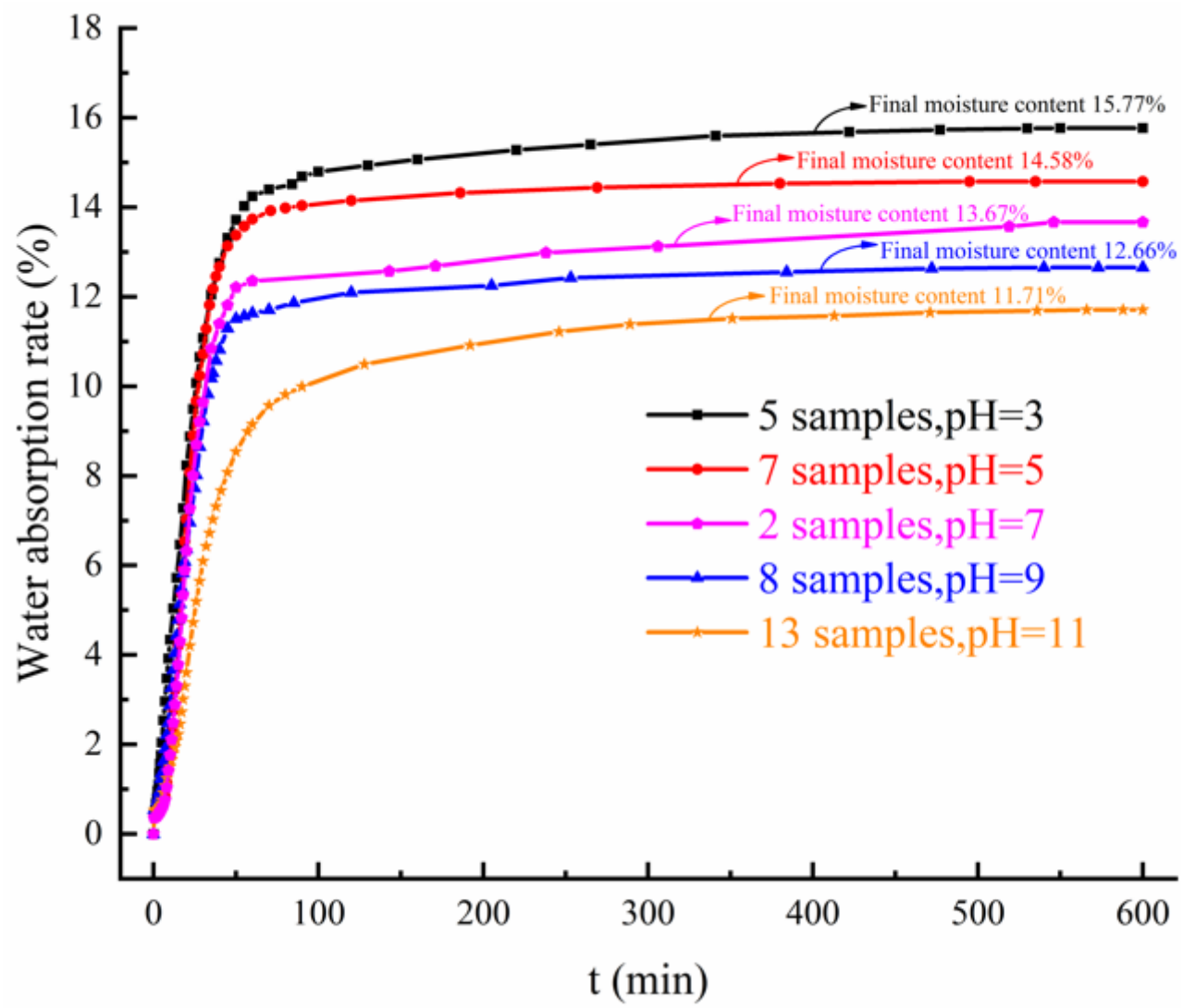

Figure 5

Changes in water absorption of mudstone samples with time under different pH values

Figure 6

Diagram of the expansion of mudstone fissures over time (a) pH=3, b) pH=5,c)pH=7,d)pH=9,e)pH=11)

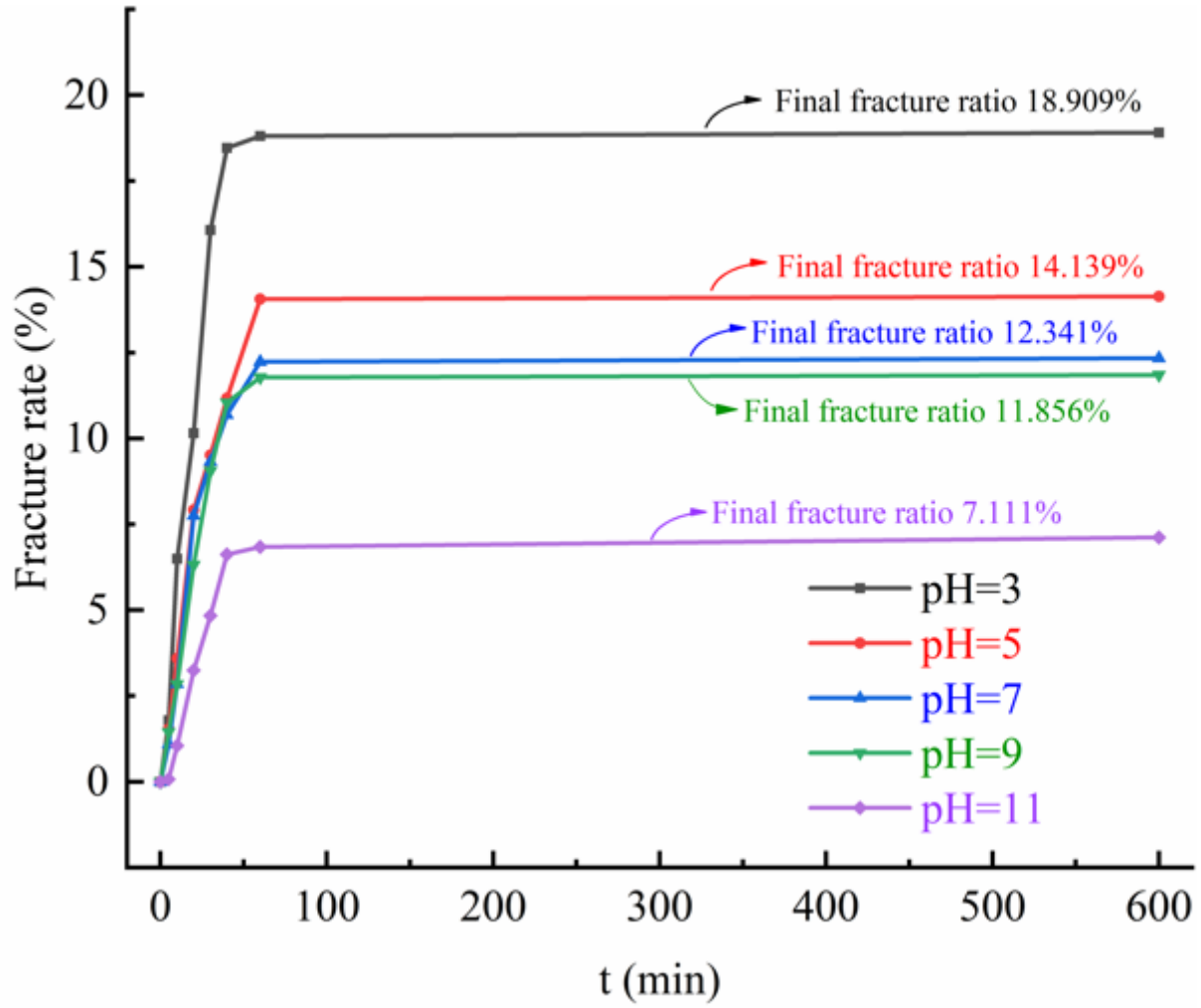

Figure 7

Mudstone fissure rate changes with time under different pH values

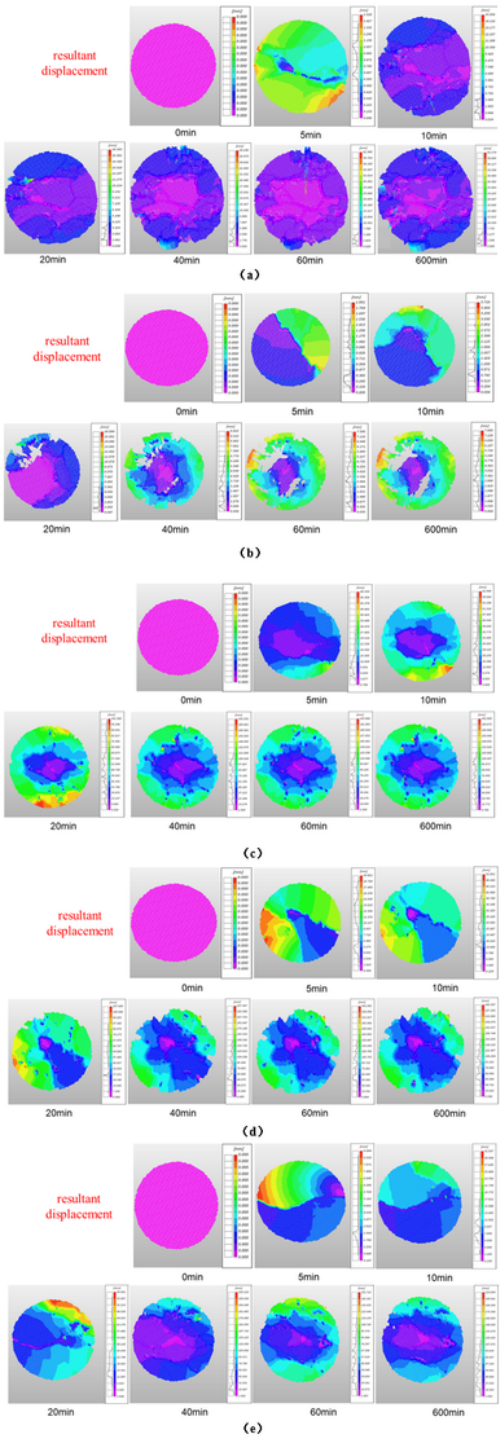

Figure 8

Moisture absorption and expansion and displacement changes of mudstone under different pH (a) pH=3, b) pH=5, c) pH=7, d) pH=9, e) pH=11)

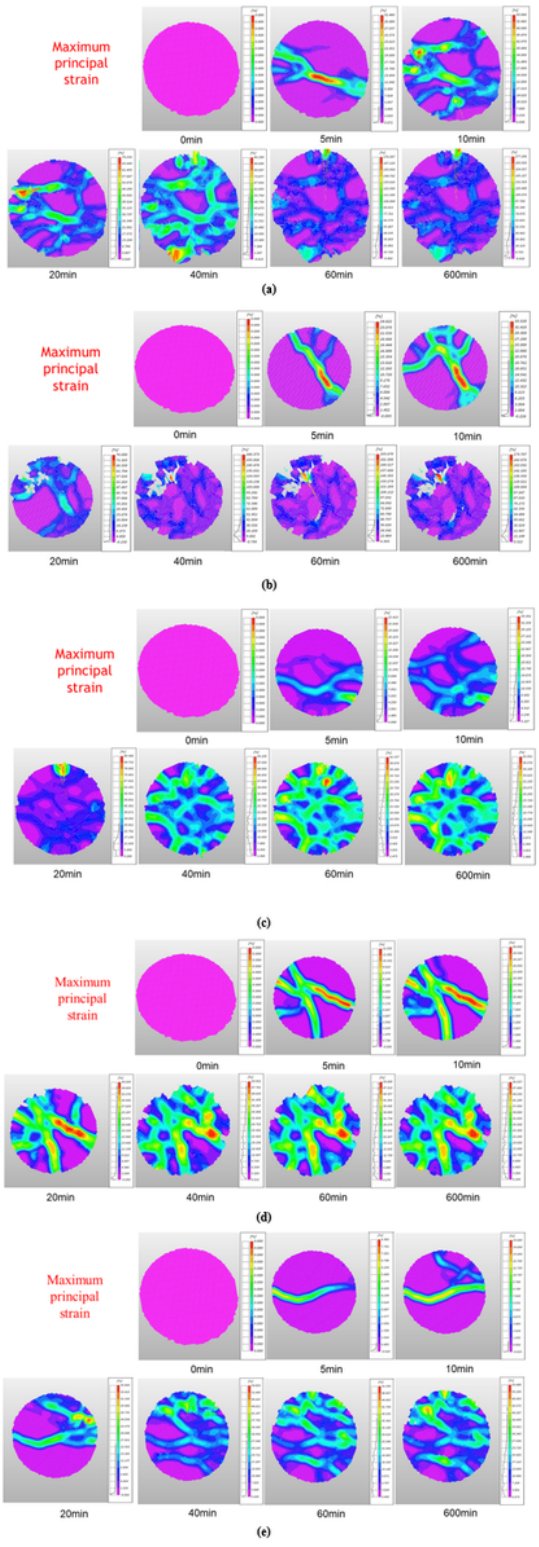

Figure 9

Variation of the maximum principal strain of mudstone swelling under different pH (a) pH=3, b) pH=5, c) pH=7, d) pH=9, e) pH=11)

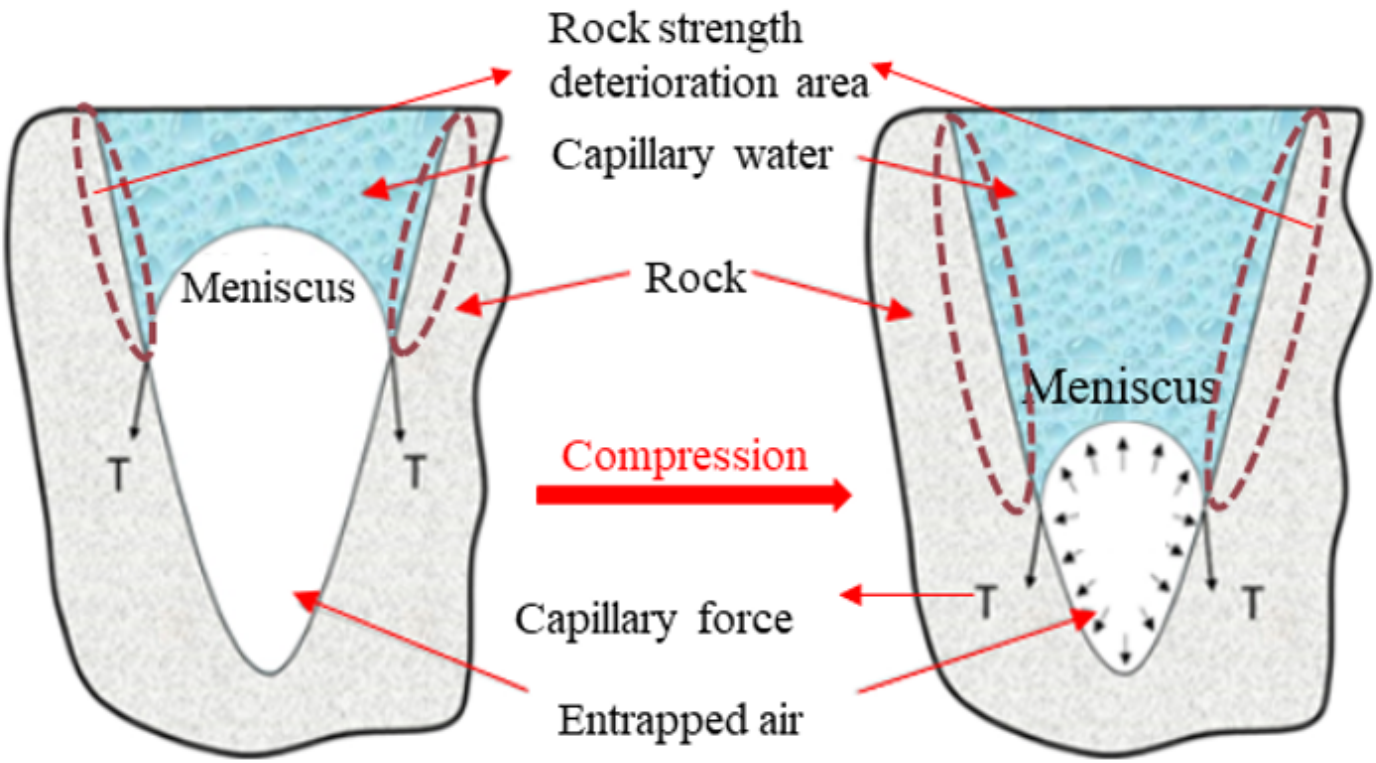

Figure 10

Simplified diagram of mudstone adsorption-wedge failure mode

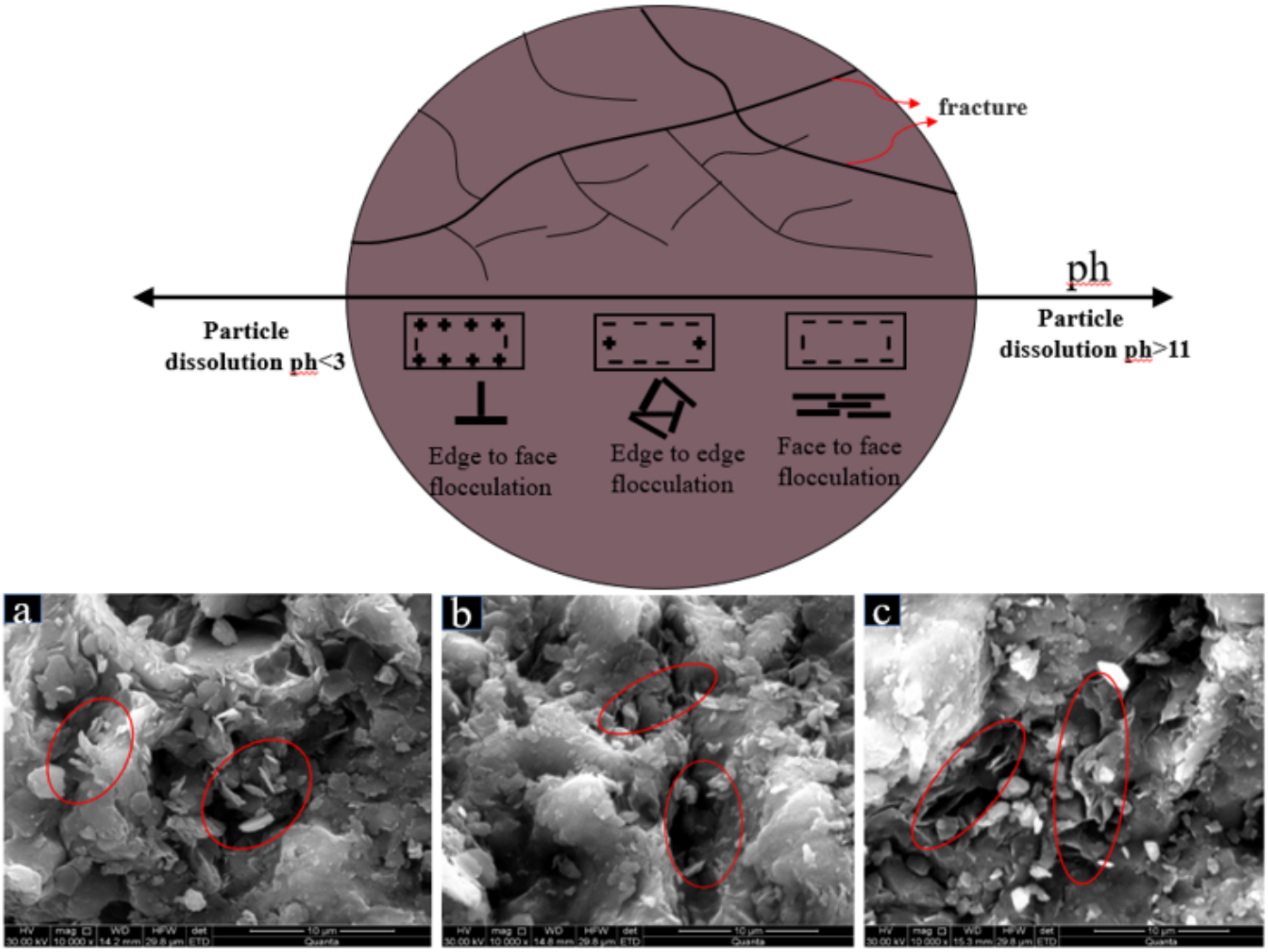

Figure 11

Clay particle association form under different pH conditions (red circle): (a) edge-to-edge flocculation, (b) edge-to-face flocculation, (c) face-to-face flocculation

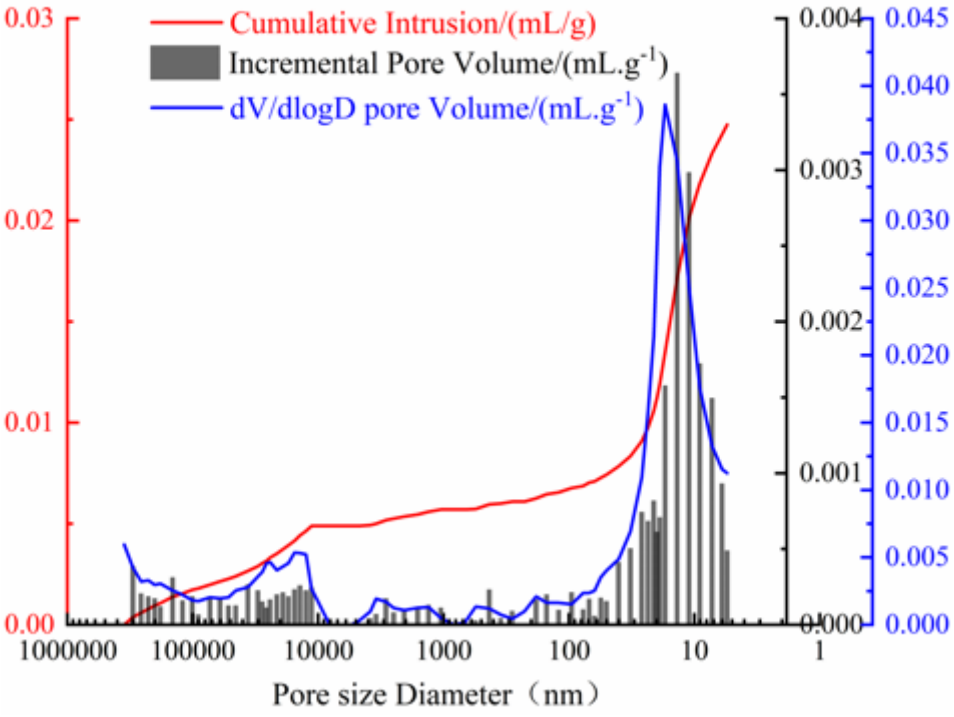

Figure 12

Mudstone pore size-pore volume distribution under the condition of pH=3

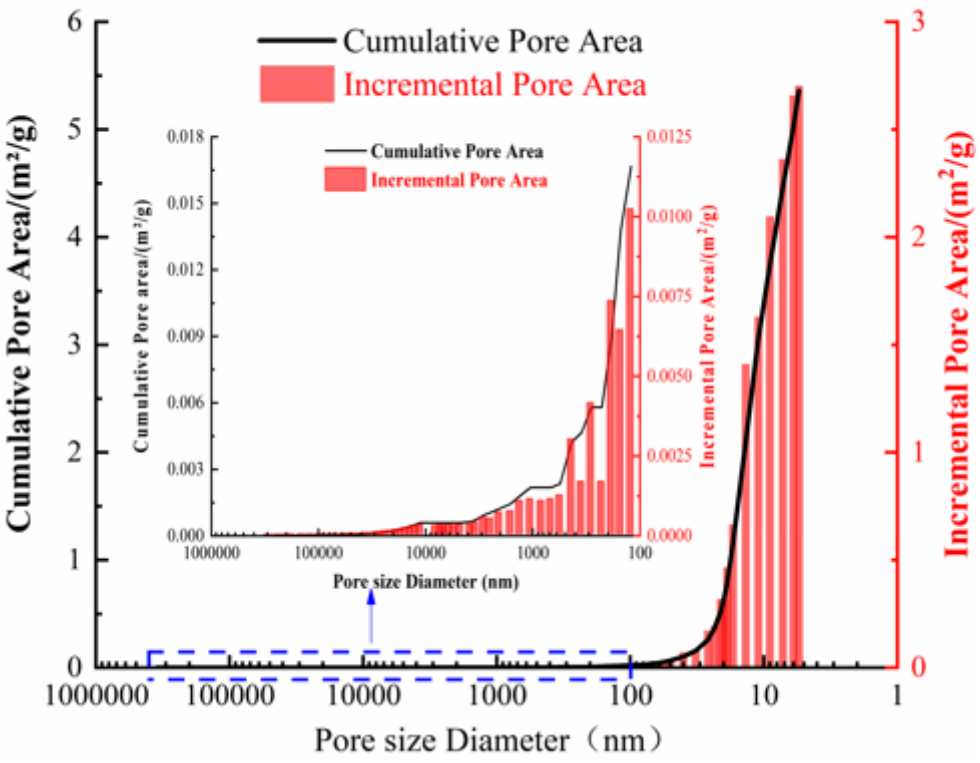

Figure 13

Mudstone pore size-area distribution under the condition of pH=3

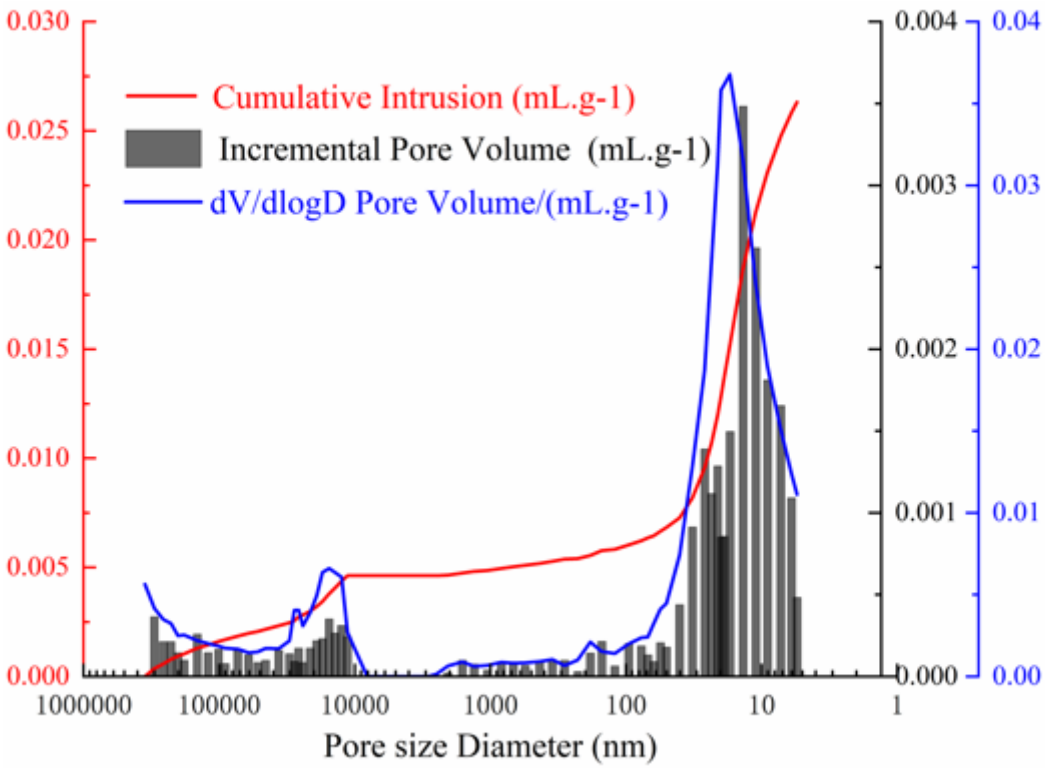

Figure 14

Mudstone pore size-pore volume distribution under the condition of pH=7

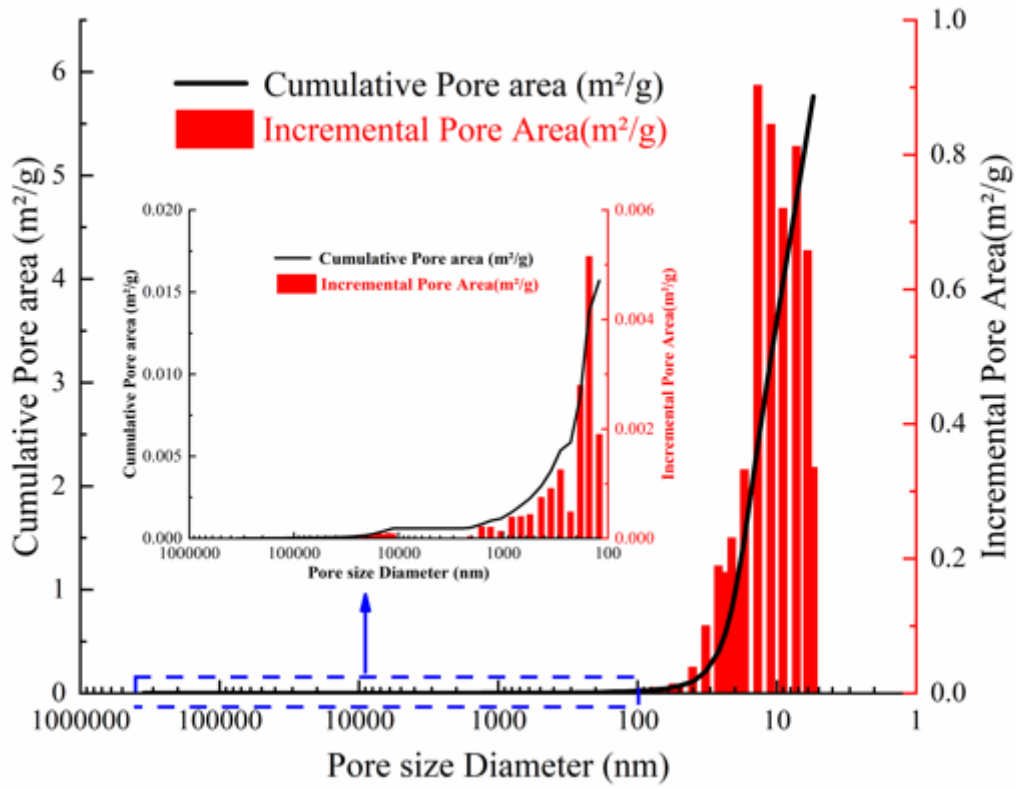

Figure 15

Mudstone pore size-area distribution under the condition of pH=7

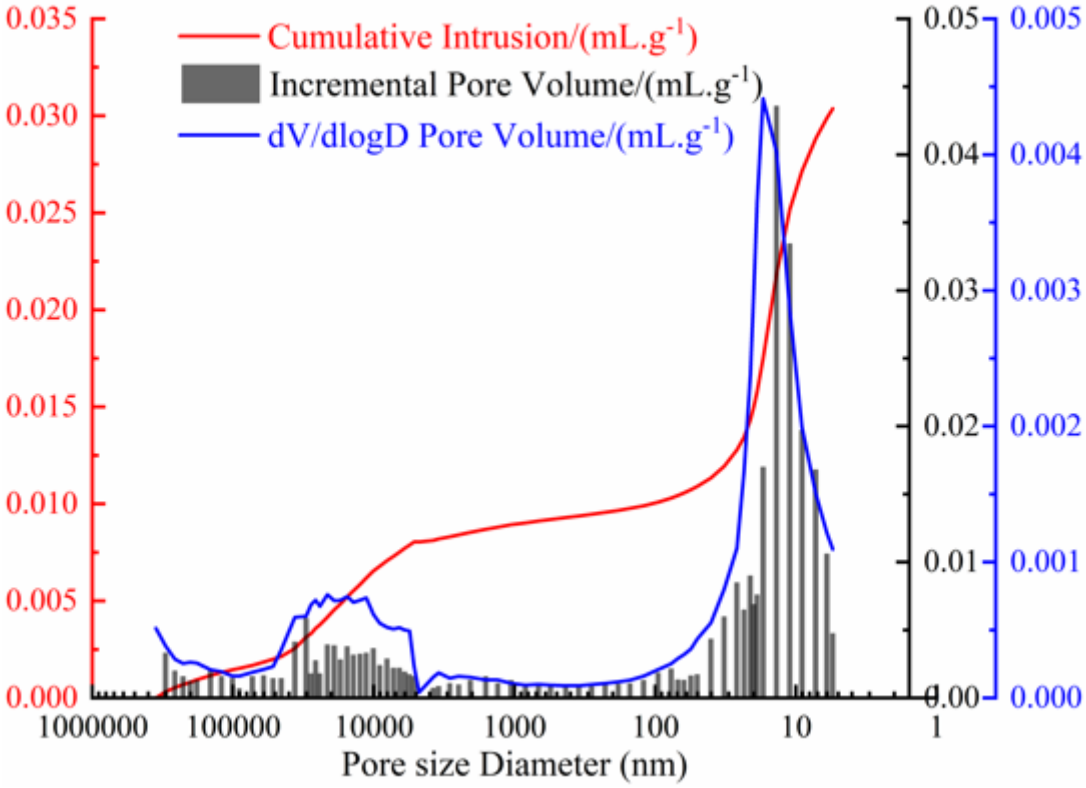

Figure 16

Mudstone pore size-pore volume distribution under the condition of pH=11

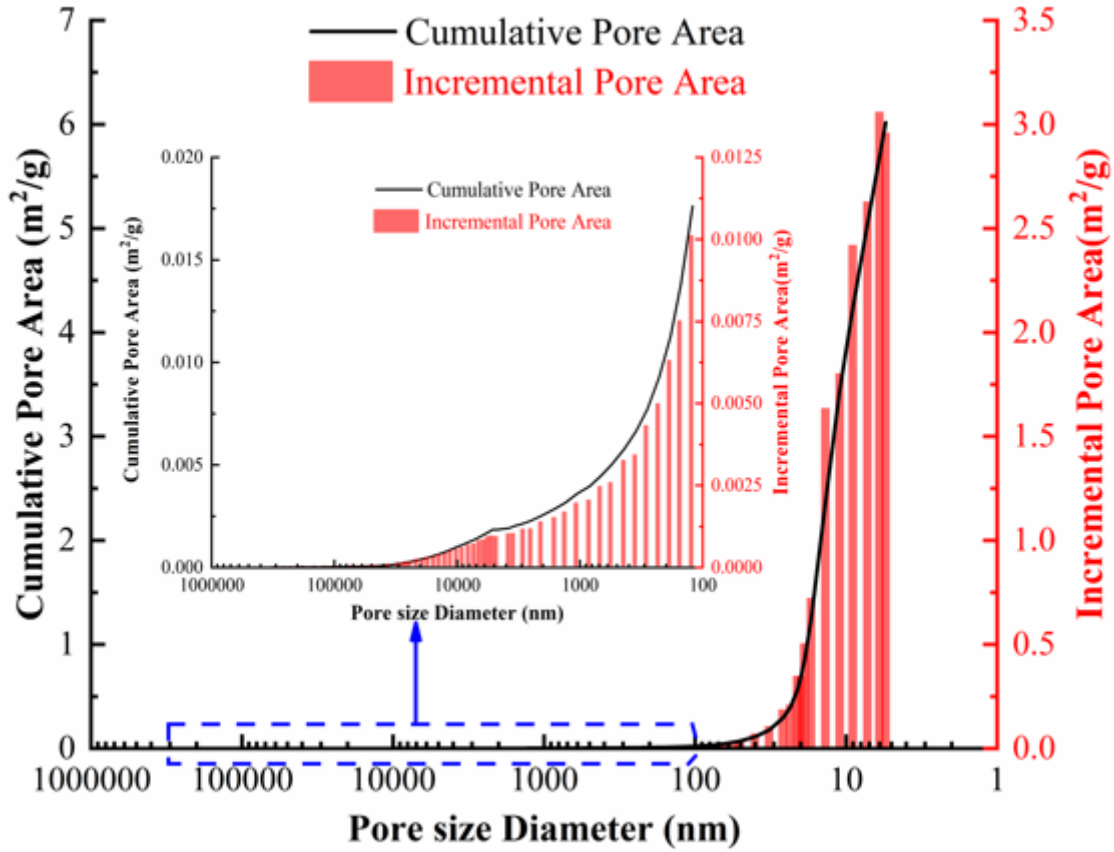

Figure 17

Mudstone pore size-area distribution under the condition of pH=11